

Population synthesis of radio and γ -ray millisecond pulsars from the Galactic disk

Sarah A. Story

*Hope College, Department of Physics, 27 Graves Place
Holland, MI 49423-9000*

inertialtensor@gmail.com

Peter L. Gonthier

*Hope College, Department of Physics, 27 Graves Place
Holland, MI 49423-9000*

gonthier@hope.edu

and

Alice K. Harding

*NASA Goddard Space Flight Center, Laboratory for High Energy Astrophysics
Greenbelt, MD 20771*

harding@twinkie.gsfc.nasa.gov

ABSTRACT

We present results of a population synthesis of millisecond pulsars from the Galactic disk. Excluding globular clusters, we model the spatial distribution of millisecond pulsars by assuming their birth in the Galactic disk with a random kick velocity and evolve them to the present within the Galactic potential. We assume that normal and millisecond pulsars are standard candles described with a common radio luminosity model that invokes a new relationship between radio core and cone emission suggested by recent studies. In modeling the radio emission beams, we explore the relativistic effects of time delay, aberration and sweepback of the open field lines. While these effects are essential in understanding pulse profiles, the phase-averaged flux is adequately described without a relativistic model. We use a polar cap acceleration model for the γ -ray emission. We present the preliminary results of our recent study and the implications for observing millisecond pulsars with GLAST and AGILE.

Subject headings: radiation mechanisms: non-thermal — magnetic fields — stars: neutron — pulsars: general — γ rays: theory

1. Introduction

Gamma-ray pulsars are the brightest objects in the sky above 100 MeV and the only identified GeV Galactic sources. Although there are presently around 1700 known radio pulsars, only a relatively small fraction of these are detected at higher energies. The EGRET detector on the Compton Gamma-Ray Observatory (CGRO) detected six γ -ray pulsars with high confidence (Thompson 2004), five of which were known radio pulsars. In addition, there were a few γ -ray pulsars detected with lower confidence, one of which was the millisecond PSR J0218+4232. The Large Area Space Telescope (GLAST), set for launch in late 2007, will have a sensitivity about 30 times better than that of EGRET and is expected to detect many more γ -ray pulsars.

Population synthesis can predict the number of expected γ -ray pulsar detections, but the results are highly model-dependent. As a consequence of this sensitive model dependence, the number of γ -ray pulsars that GLAST does detect, especially the ratio of radio-loud to radio-quiet pulsars, will be an excellent discriminator between γ -ray models. Using polar cap models to describe the γ -ray emission, population synthesis studies of Gonthier et al. (2002, 2004) have estimated that GLAST should detect several hundred pulsars. Population synthesis studies for outer gap models (Jiang & Zhang 2006; Harding, Grenier & Gonthier 2006) generally predict fewer radio-loud γ -ray pulsars and a much higher ratio of radio-quiet to radio-loud pulsars. These studies evolved neutron stars in the Galaxy from birth distributions of period, magnetic field, position and space velocity, but excluded the population of millisecond pulsars (MSPs). Since MSPs are thought to be recycled through spin-up by accretion from a binary companion, their evolution is somewhat more complicated.

Because of their very short periods, MSPs can have spin-down luminosities that are comparable to those of young pulsars and therefore should be sources of high-energy photons. Indeed, a much higher fraction of the total radio MSP population (around 225) have been detected as X-ray sources (around 60, including Globular Cluster pulsars) compared to normal pulsars. The pulsed X-ray spectra of most MSPs in the Galactic plane are dominated by non-thermal emission (Kuiper et al. 2003), so these sources must be accelerating particles to high energy. Polar cap models predict that MSPs should produce a high-energy emission component due to curvature radiation up to energies around 50 GeV (Harding, Usov, & Muslimov 2005; Lou, Shibata, & Melrose 2000). Outer gap models also predict that MSPs could produce high-energy emission from particles moving downward toward the stellar surface from the outer gap (Zhang & Cheng 2003). Predictions for the number of γ -ray MSPs in globular clusters have been discussed by Wang, Jiang, & Cheng (2005).

Studies of the radio characteristics of MSPs indicate some differences with those of the normal pulsar population. Kramer et al. (1998) and also Bailes et al. (1997) found that

MSPs are somewhat less luminous than normal pulsars. However, these studies compare the pseudo-luminosities, i.e. the observed radio flux times the square of the distance, which are dependent on solid angle and observer viewing angle, and do not address real luminosities. These studies also found that the beam radii of MSPs, although larger on average than those of normal pulsars, are smaller than expected by an extrapolation of beam radii with a $P^{-1/2}$ dependence of the normal pulsars population. The average MSP beam widths seem to reach a saturated value of around $30^\circ - 50^\circ$, whereas the extrapolated value is greater than 100° . We will argue however that relativistic effects (Harding, Grenier & Gonthier 2006) may strongly influence the shape of MSP profiles. MSP pulse profiles have considerably larger duty cycles than normal pulsars and the beaming fractions are thought to be around 75% (Kramer et al. 1998). The profiles were originally thought to have more complex structure, a feature that was attributed to the presence of multipole field components, possibly induced by the accretion phase (Krolik et al. 1991; Kramer et al. 1997). But the observations of Kramer et al. (1998) do not support this claim and show that MSP profiles display in general only marginally more complexity. The more observable details afforded by the larger duty cycles make the profiles seem more complex with the large beams increasing the chance of detecting emission from both poles. Additionally, the emission height dependence on frequency (radius-to-frequency mapping) is less strong, and this is understandable since the MSP magnetospheres are much smaller. In general, MSP radio profiles are consistent with an expanded version of normal pulsar emission on open dipole field lines, with the smaller widths being attributed to emission occurring only on a subset of the open field lines or to relativistic distortions of the beam.

We present in this paper new results of a population synthesis of MSPs born within the Galactic disk. In this study we define MSPs as those pulsars with period derivatives $\log(\dot{P}) < -19.5 - 2.5 \log(P)$. This criterion includes the binary pulsars J1744-3922 and B0655+64 with periods of 172.4 ms and 195.7 ms, respectively, but excludes the binary pulsar J1711-4322 with a period of 102.6 ms. By means of a Monte Carlo population code, we treat them as point particles and evolve their trajectories, periods and period derivatives from their birth (at time of their last spin-up phase) forward in time to the present. We exclude MSPs in globular clusters from our study. After determining a present-day spatial equilibrium distribution, we assign radio and γ -ray characteristics to each MSP and then filter its properties for detection through a select group of radio surveys and the γ -ray instruments EGRET, AGILE and GLAST. We normalize the number of simulated radio MSPs to the number detected by the group of radio surveys, allowing us to predict the number of radio-loud and radio-quiet γ -ray MSPs detected by EGRET, AGILE and GLAST.

2. Selected Radio Surveys

We recently added the Swinburne Intermediate Latitude survey to our selected group of radio surveys used in previous studies. Of the ten surveys, six of them, Arecibo 2 & 3, Greenbank 2 & 3, Molongo 2 and Parkes 2, have an observing frequency around 400 MHz, and four surveys at 1400 MHz include Parkes 1, Jodrell Bank 2, Parkes Multibeam, and Swinburne Intermediate Latitude. In our computer code, we use the characteristics of these ten surveys to determine the minimum flux threshold for each simulated pulsar (for details see Gonthier et al. (2002, 2004)) at the observing frequency of the survey. While we recognize that some of these radio surveys were not very sensitive to the detection of MSPs, we include them to confirm null detections. When the simulated radio flux is below the flux threshold S_{min} of all the radio surveys that potentially are viewing the simulated pulsar, we refer to the pulsar as being radio-quiet. Otherwise, the pulsar is radio-loud. These characterizations are relative to the sensitivity of the surveys and are not addressing the nature of the emission process. We then are restricted to comparing the characteristics of the pulsars simulated by our computer code to those MSPs detected by this select group of radio surveys, excluding MSPs detected only by other surveys.

3. Kick Velocity and Equilibrium Spatial Distribution

We assume exponential spatial distributions of the form described in the study of Paczyński (1990), but using a scale height parameter above the Galactic plane of 200 pc for MSPs in contrast to 75 pc used in our simulations for NPs. We use a Maxwellian distribution with a characteristic width of $\sigma_v = 70$ km/s to describe the supernova kick velocity at birth from the study of Hobbs et al. (2005), resulting in an average velocity of 110 km/s. We assume a uniform birth rate back in time to 12 Gyr. To determine an equilibrium spatial distribution, we evolved a group of 40,000 neutron stars to the present without making any selections. As in our recent studies, Gonthier et al. (2007) and Story et al. (2006), we use the Galactic potential (mass model 2) of Dehnen & Binney (1998) (W. Dehnen private communication) to evolve the trajectories of MSPs using a 5th order Cash-Karp Runge-Kutta routine (Press et al. 1992). While MSPs are born in binary systems, we have not attempted to simulate the evolution of the binary system, but rather treat the system as a point particle and evolve it within the Galactic potential. With low kick velocities, the MSPs remain bound to the Galaxy and achieve normalized equilibrium distributions in Galactic radius (R) and Galactic height (Z) shown in Figure 1 as solid curves with the initial distributions represented by the dotted curves.

Fitting the equilibrium distributions results in radial and out-of-plane scale heights of 4.2

kpc and 0.50 kpc, respectively. The Z scale height of 0.50 kpc is in good agreement with the one obtained by Cordes & Chernoff (1997) of 0.50 kpc and with the recent determinations of the scale heights of low mass X-ray binaries (LMXB) by Grimm, Gifanov & Sunyaev (2002) of 0.41 kpc. In subsequent calculations, we use these equilibrium distributions to randomly select the present-day spatial distribution of MSPs within the Galaxy. In choosing the R and Z values of MSPs from such an evolved distribution rather than evolving each MSP from its birth location, we ignore any dependence of evolved R and Z on MSP age.

According to Shklovskii (1970), the transverse motion of a pulsar causes a change in the pulsar’s detected period. Due to the Doppler effect, an increase in the pulsar’s period derivative is observed. The contribution to \dot{P} due to this effect is given by (Manchester 1999)

$$\dot{P} = 2.43 \times 10^{-27} \left(\frac{P}{\text{ms}} \right) \left(\frac{\mu}{\text{mas/yr}} \right)^2 \left(\frac{d}{\text{pc}} \right), \quad (1)$$

where P is the pulsar period, μ is the proper motion, and d is the distance. For MSPs, whose period derivatives are extremely small, this effect can increase period derivatives significantly, in some cases by as much as 90% as noted by Toscano et al. (1999) who have also included the smaller effects of Galactic rotation and vertical acceleration. In this study, we only include the Shklovskii effect due to the proper motion of the simulated pulsar.

4. Magnetic Field and Initial Period

While it may be that the magnetic field of MSPs decays slowly, we have assumed a constant field during their lifetime. However, due to selection effects, the observed field distribution will differ from the initial distribution. We explored power laws with various indices to characterize the distribution of pulsar surface magnetic field at the birth line. While Cordes & Chernoff (1997) preferred a power law with an index of -2, the group of 22 MSPs used in their study had smaller magnetic fields. For the group of 56 MSPs in this study, we find a preferred index of -1 with a normalized distribution of the form

$$n(B_8) = \frac{1}{B_8 \ln \left(\frac{B_{\text{max}}}{B_{\text{min}}} \right)}, \quad (2)$$

where B_8 is in units of 10^8 G. We choose a $B_{\text{min}} = 1$ and a $B_{\text{max}} = 10^4$ that provides the best agreement between various simulated and detected distributions.

Having the magnetic field for a simulated MSP, we can obtain its initial period with a spin-up relation. Alpar et al. (1982) and similarly Bhattacharya & van den Heuvel (1991)

found that for recycled pulsars spun up by accretion at the Eddington limit from a binary companion, the initial period is estimated by the expression

$$P_o = 0.3B_8^{6/7}\text{ms}, \quad (3)$$

which can be rewritten as a birth line in the $\dot{P} - P$ diagram by the form

$$\log \dot{P}_o = \frac{4}{3} \log P_o - 15.4, \quad (4)$$

where the period is in seconds and the period derivative is $\text{s} \cdot \text{s}^{-1}$. Having the magnetic field, the initial period, and the age, we can determine the present period and period derivative of the MSP assuming a pure dipole spin down. However, recent studies of LMXBs where the spin periods of accreting neutron stars were measured have allowed the estimation of the surface magnetic fields. Lamb & Yu (2005) conclude that the general properties of LMXBs can be understood if the accretion rates range from the Eddington critical accretion rate to 5×10^{-4} times that rate. These different accretion rates lead to different birth lines in the $\dot{P} - P$ diagram. To incorporate a distribution of accretion rates, we have included an approximate procedure in which we dither the intercept of the following birth line

$$\log \dot{P}_o = \frac{4}{3} \log P_o - 14.9 - \delta, \quad (5)$$

where the dithering parameter δ varies from 0 to 2.8. The birth line can be reformulated by the expression

$$P_o = 0.18 \times 10^{3\delta/7} B_8^{6/7} \text{ms}. \quad (6)$$

The extremes of the dithering parameter δ represent the approximate Eddington accretion critical rate and 5×10^{-4} times that rate (see figure 4 in Lamb & Yu (2005)). While we explored a Gaussian distribution of the dithering parameter, we obtain better agreement with a ramp distribution that increases by a factor of 4 between 0 and 2.8. With the magnetic field randomly selected from the distribution of Equation 2, we then use Equation 6 to obtain the initial period of the simulated MSP. However, we impose a minimum initial period of $P_{o_{\min}} = 1.3 \text{ms}$ in accord with the RXTE studies of LMXBs by Chakrabarty (2005). Having randomly determined the pulsar's age assuming a uniform birth rate, we spin the pulsar down to obtain the present period and period derivative assuming constant magnetic surface field. A constant magnetic field used in this study of MSPs is in contrast to the assumption of magnetic field decay in our simulations of NPs (Gonthier et al. 2002, 2004, 2007).

5. Radio Luminosity and Beam Geometry

In our previous studies of NPs (Gonthier et al. 2002, 2004, 2007), we adopted the intrinsic radio luminosity model given by the general form

$$L = L_o P^\alpha \dot{P}^\beta, \quad (7)$$

from Arzoumanian, Chernoff & Cordes (2002) (ACC) with $L_o = 2.1 \times 10^{12} \text{mJy} \cdot \text{kpc}^2 \cdot \text{MHz}$, $\alpha = -1.3$ and $\beta = 0.4$, but reduced the luminosity L_o by a factor of 60 (Gonthier et al. 2004) and by 73 (Gonthier et al. 2007) to obtain adequate agreement between the simulated birth rate, flux, and distance distributions and those detected, particularly by the Parkes Multibeam Pulsar survey (PMBPS) (see Gonthier et al. (2004)). In ACC, the predicted birth rate was 0.13 neutron stars per century. In order to obtain a birth rate near 2 neutron stars per century, we had to decrease the luminosity constant L_o . The assumed radio luminosity is directly related to the simulated neutron star birth rate. Various studies propose neutron star birth rates that span somewhat of a range. For example, the a range of birth rates from 0.9 to 1.9 per century was obtained from the analysis of PMBPS by Vranesevic et al. (2004). In a recent population synthesis, Faucher-Giguère & Kaspi (2006) estimate a larger birth rate of about 2.8 per century, whereas Lorimer et al. (2006) find 1.4 ± 0.2 per century from their analysis. More recently Gonthier et al. (2007) determined the reduction factor of the radio luminosity by normalizing the simulated neutron star birth rate to rate of Type II supernovae of 2.1 per century, following the work of Tammann, Löffler & Schröder (1994), using only the Parkes Multibeam survey, as we may have the best description of the flux threshold S_{min} for that survey (Crawford, private communication).

While the neutron star birth rate of 2.1 per century provides a constraint on the luminosity of NPs, MSPs appear in a very different region in the $\dot{P} - P$ diagram, requiring careful consideration of the period and period derivative dependence of the radio luminosity used by the population synthesis study. Often, radio astronomers refer to the radio luminosity in terms of a “pseudoluminosity” (Sd^2) determined from the radio flux S observed at a specific frequency and the pulsar distance d . One cannot generally determine the intrinsic radio luminosity of a given pulsar from the Sd^2 , even at a given frequency, as the detected average flux is strongly dependent on the viewing geometry. However, if the number of detected pulsars in a group is large, one might be justified in assuming that the emission region of the group of pulsars is completely sampled in a random fashion. Therefore, the detected Sd^2 would be proportional to the intrinsic luminosity of the group of pulsars if the surveys represented an unbiased sample of the true flux distribution. However, since radio surveys necessarily sample the high end of the flux distribution, inferring the intrinsic luminosities of pulsars is difficult at best. In addition, selection effects of the radio surveys may be different for NPs and MSPs, and these effects do influence the sampling of the emission region. For

example, the width of the pulse profile is used in the determination of the flux threshold S_{\min} for each radio survey; therefore, one would expect that narrow pulse profiles or larger inclination angles are preferably detected. Regardless of these effects, such comparisons are important in characterizing differences between NPs and MSPs. Kramer et al. (1998) compared the average $\log(Sd^2)$ ($\text{mJy} \cdot \text{kpc}^2$) of a group of MSPs with that of a group of NPs and found that the mean $\log(Sd^2)$ values for their groups of 31 MSPs and of 369 NPs of 0.5 ± 0.2 and 1.50 ± 0.04 , respectively. The authors conclude that MSPs and NPs have very different radio luminosity distributions. Since this study was performed, the NE2001 distance model (Cordes & Lazio 2002) was developed. We use the pulsar distance given by the NE2001 model unless the distance has been determined by other more accurate methods. After this distance correction and using the 1400 MHz fluxes in the ATNF catalogue that have a recorded uncertainty (Lorimer et al. 1995; Kramer et al. 1998; Lorimer et al. 2006; Manchester et al. 2001; Hobbs et al. 2004; Kramer et al. 2003; Faulkner et al. 2005, 2004; Morris et al. 2002; Stairs et al. 2005), we find average $\log(Sd^2)$ values of 0.38 ± 0.15 for our select group of 39 MSPs (24 with S1400 fluxes) and 1.17 ± 0.02 for a group of 1102 NPs (869 with S1400 fluxes (references in ATNF catalogue)) detected by Parkes Multibeam and the Swinburne Intermediate Latitude surveys. The uncertainties are just the statistical error in the mean and do not take into account the error in the fluxes and distances. Subtle selection effects may be introduced within the context of a population statistics study with a group of surveys that have different sensitivities. As a result, it may be inappropriate to compare these mean $\log(Sd^2)$ values with those from Kramer et al. (1998) because of the different samples of pulsars. The MSPs recently discovered by the Parkes Multibeam and Swinburne surveys are not only more distant but also weaker with effectively smaller $\log(Sd^2)$. We have chosen to reproduce the $\log(Sd^2)$ values of the normal pulsars and MSPs detected by these surveys to constrain our luminosity model.

We adjust our intrinsic radio luminosity model such that the simulated mean $\log(Sd^2)$ values approximately match both the mean values of 0.38 ± 0.15 for MSPs and 1.17 ± 0.02 for NPs detected by both the Parkes Multibeam and the Swinburne Intermediate Latitude surveys. We find that the exponents of the period (α) and period derivative (β) dependence of the luminosity are not uniquely constrained to specific values but are correlated with each other. We find better agreement between the various simulated distributions for NPs with values of $\alpha = -1.05$ and $\beta = 0.37$. The coefficient of the luminosity is adjusted to give a birth rate of 2.1 neutron stars per century using the Parkes Multibeam and the Swinburne Intermediate Latitude surveys.

We were able to find a common radio luminosity that provides adequate results for both NPs and MSPs, given by the expression

$$L = 1.76 \times 10^{10} P^{-1.05} \dot{P}^{0.37} \text{mJy} \cdot \text{kpc}^2 \cdot \text{MHz}. \quad (8)$$

In this study, we assume that the radio emission originates from a single core beam and a single cone beam axially aligned with the magnetic field from each pole of the star and isotropically distributed in the sky. As indicated by Kramer et al. (1998), the profiles of MSPs display similar structure to those of NPs, suggesting that the core or central beam and the conal beam make similar contributions to NP and MSP profiles. However, as discussed later, due to the rapid rotation of MSPs, relativistic effects are more evident in the pulse profiles of MSPs than in those of NPs (Xilouris et al. 1998). We use the same description for the core beam as in our past study of Gonthier et al. (2004), but we replace the geometry of the cone beam from the Mitra & Deshpande (1999) with the description of Kijak & Gil (1998, 2003) having the form

$$\rho_{\text{cone}} = 1.24^\circ r_{\text{KG}}^{1/2} P^{-1/2}, \quad (9)$$

which describes the characteristic width of the conal beam at 0.1% of the peak intensity of the profile assuming that the edges of the pulse are along the last open field line. They find that the altitude of the emission r_{KG} in stellar radii is given by

$$r_{\text{KG}} = 40 \nu_{\text{GHz}}^{-0.26} \dot{P}_{-15}^{0.07} P^{0.3}, \quad (10)$$

where \dot{P}_{-15} is in units of $10^{-15} \text{ s} \cdot \text{s}^{-1}$. In this formulation, the overall period dependence of the characteristic width of the conal beam is $\rho_{\text{cone}} \sim P^{-0.35}$, reproducing well the trend observed for NPs and MSPs (Kramer et al. 1998; Kramer 2002).

In the formulation of a Gaussian conal beam, the characteristic width ρ_{cone} requires the specification of the radius $\bar{\theta}$ and width w_e of the annulus of the beam. The characteristic width of Kijak & Gil (1998, 2003) is for 0.1% of the peak intensity making $\rho_{\text{cone}} = \bar{\theta} + 2.63w_e$. Within such a model, one is free to specify some form for either $\bar{\theta}$ or w_e . We adopted $w_e = 0.18\rho_{\text{cone}}$ in our study of both normal and MSPs. We find that the population statistics are not very sensitive to the choice of this value, which we have arrived at from our study of three peak pulse profiles of radio pulsars. In our study of the characteristics of core and cone beams of about 20 radio pulsars whose profiles have three peaks, we found (Gonthier et al. (2006) and in preparation) that the ratio of core-to-cone peak fluxes does not follow the P^{-1} dependence suggested in the work of ACC. In the ACC model, the profiles of MSPs are dominated by the central core beam, so that even at small impact angles the conal beam would not be seen. As seen in the study of Kramer et al. (1998), similar complexity is manifested in the MSPs profiles as in profiles NPs, indicating that the conal beam is quite prominent. Recent polarimetry studies of young radio pulsars also call the ACC core-to-cone ratio into question. Crawford, Manchester & Kaspi (2001) and Crawford & Keim (2003) measured the radio polarization of nine pulsars, six of which had characteristic ages less than 100 kyr. They found that the profiles of all the young pulsars indicate a significant degree of linear polarization and a low degree of circular polarization, which is a traditional

feature of conal emission. In this study, the two older pulsars with characteristic ages greater than 1 Myr do not show any degree of polarization. They conclude, as did Manchester (1996), that the profiles of young short period pulsars tend to be characterized by partial cones. Similarly, in a more recent study Johnston & Weisberg (2006) measured polarization profiles of 14 young pulsars with ages < 75 kyr. They found that the profiles are dominated by linear polarization, suggesting that the core beam is weakly manifested, if at all. Because of these inconsistencies, we have reassessed the relationship between the core and cone beams (Gonthier et al. (2006)), using three-peak normal pulsars and a few three-peak MSPs. In our three-peak pulsar study, we find for the ratio of peak fluxes a power-law dependence with a break in period at about 0.7 s having the approximate form

$$r = \begin{cases} 25P^{1.3}\nu_{\text{GHz}}^{-0.9}, & P < 0.7\text{s} \\ 4P^{-1.8}\nu_{\text{GHz}}^{-0.9}, & P > 0.7\text{s}. \end{cases} \quad (11)$$

Hence in this model, short period pulsars are much less core dominated than in the ACC model. The model does not distinguish between young short-period pulsars and MSPs, although there is evidence (Kramer et al. (1999)) that the ratio of core-to-cone peak fluxes may be different for a young pulsar and a MSP with the same period. The shapes of MSP profiles are complicated by relativistic effects, but due to the wide emission beams, contributions from both poles are often seen in the profiles, making the analysis of the viewing geometry and conal widths difficult. With this model, we do accommodate more complex pulse profiles for short period pulsars than in the ACC model.

In describing the core and cone angle-integrated spectra, we assume indices of -2.36 and -1.72, respectively. While these indices are not measurable, they are related in a complex fashion, due to selection effects, to the measured spectral indices. Using these values, our simulation gives a flux-averaged spectral index of -1.80 ± 0.05 for MSPs. Within our select group of surveys, we find 20 MSPs within the ATNF catalogue whose spectral indices have recorded uncertainties (Toscano et al. 1998; Lorimer et al. 1995) with a mean of -1.89 ± 0.10 . Kramer et al. (1998) found a mean spectral index of -1.8 ± 0.1 for a group of 32 MSPs. They also point out that MSPs have significantly steeper mean spectral indices than NPs. For a group of 346 NPs, they find a mean spectral index of -1.60 ± 0.04 . In our simulation, we found it necessary to have softer angle-integrated spectral indices for the core and cone beams of NPs, resulting in a mean spectral index of -1.58 ± 0.01 . This value agrees well with the mean spectral index of -1.66 ± 0.04 for the 245 NPs with indices that have recorded uncertainties in the ATNF catalogue (references therein).

Adopting this radio luminosity and beam geometry model, we attempt to describe radio emission properties from both NPs and MSPs (Gonthier et al. 2007; Harding, Grenier & Gonthier 2006). The success of this radio model is remarkable in describing the physical luminosities of

both NPs and MSPs, given the range of three decades in period and seven decades in period derivative between NPs and MSPs. However, it is clear that there are many complexities that may not modeled correctly and that the population synthesis study may not be very sensitive to various characteristics of the beam geometry.

6. Relativistic Effects in the Radio Profiles

Because of their rapid rotation, MSPs can display very different features in their pulse profiles than those observed in the profiles of NPs. These features can be partly understood in terms of the relativistic effects of aberration, time delay and the sweep back of the retarded dipole field (Dyks & Harding 2004; Dyks, Harding & Rudak 2004). The shorter the pulsar period, the more dramatically these effects are manifested in the profiles. According to Equation 10, the conal emission of pulsars with short periods occurs at high altitude relative to the light cylinder radius. For MSPs the altitude of emission for the cone beams (r_{KG}) is $\sim 0.2 - 0.6 R_{LC}$. The combined effects of time delay and aberration result in a shift in phase of the conal beam. Deformations in the shape of some profiles of MSPs are a result of the distortion of the open field volume of the retarded dipole (Dyks & Harding 2004). While relativistic effects are important in understanding the shape of the profile and in studying correlation with high-energy profiles, in a recent study (Story et al. 2006), we find that the phase-averaged flux is very similar for relativistic and nonrelativistic emission. Since in population statistics studies, the average flux of the profile is the determining parameter that is compared to the threshold of each radio survey, we have neglected these effects in this study.

7. Gamma-ray Luminosity and Beam Geometry

Because of the lack of a theoretical understanding of the mechanism that produces the radio emission, the radio emission model is phenomenological by nature. On the other hand, the γ -ray emission models are motivated by theory. Two competing γ -ray emission models, the polar cap and outer gap models, assume different locations in the magnetosphere where the acceleration of charge occurs. In the outer gap model, the acceleration of charge takes place in vacuum gaps formed along the last open field line, between the null surface and the light cylinder. While we are beginning to incorporate an outer gap in our simulations (Harding, Grenier & Gonthier 2006), treating it on the same footing as the polar cap model using the same group of evolved neutron stars and selection criteria, we use only the polar cap model in this study of MSPs. Recent outer gap models for MSPs (Zhang & Cheng 2003)

actually assume that the high-energy emission originates not from the outer gap but near the neutron star, from particles flowing down from the gaps, and thus would have a very different high-energy emission geometry from that of normal pulsars.

Two regions in the $\dot{P} - P$ diagram, separated by the curvature radiation (CR) pair death line, differentiate the γ -ray luminosities and beam geometries within the polar cap model. Pulsars above the CR line can produce CR photons that are energetic enough to pair produce in the strong magnetic field above the neutron star surface. The CR-initiated pair cascades have sufficient multiplicity to fully screen the parallel electric field everywhere except in the slot gap along a narrow region near the last open field line where the primary particles are accelerated along unscreened electric field lines. Recent studies (Muslimov & Harding 2003, 2004) of the emission above the CR pair death line in the polar cap model have provided a framework for understanding γ -ray emission from the slot gap. The electrons in the low altitude slot gap initiate pair cascade emission, which was incorporated in our simulations of Gonthier et al. (2004, 2007). In addition, Muslimov & Harding (2004) find that the primary particles along the last open field lines can be accelerated to high altitudes as the potential in the slot gap remains unscreened and the emission beam forms a characteristic caustic component (Dyks & Rudak 2003). In recent population studies of NPs, we have begun to include both the low and high altitude emission geometries (Gonthier et al. 2007; Harding, Grenier & Gonthier 2006) and both are included in this study for those simulated MSPs above the CR line.

However, as one can see in Figure 2, all the MSPs with the exception of one lie below the CR line where curvature radiation no longer produces pairs. These pulsars can produce much weaker pair cascades through inverse Compton scattering radiation. When pulsars are no longer able to produce abundant pair cascades, they do not form slot gaps above the polar cap Muslimov & Harding (2003) as the parallel electric field is not screened on all open magnetic field lines. As the γ -ray energies are below the pair threshold, the curvature radiation from the primary electrons escapes out to infinity along all open field lines. In this pair-starved polar cap model, the primary particles continue to accelerate and radiate to high altitudes above the polar cap out to the light cylinder along all the open field lines. However, CR emitted by the particles can be inhibited by resonant cyclotron absorption of radio emission (Harding, Usov, & Muslimov 2005) where synchrotron radiation is more efficient particle energy loss mechanism than CR. Since synchrotron photons usually have lower energies than curvature photons, we have not included this mechanism in the pair-starved model in this study. The CR emission model below the CR pair death line used in this study is developed from the work by Harding, Usov, & Muslimov (2005).

The inclination angle α and the viewing angle ζ determine which open field lines are

sampled by the line of sight. As illustrated in Figure 3, the line of sight intersects tangentially a particular open field line with a radius of curvature ρ_c at a radial distance r and polar angle θ . The open field lines are defined within the polar cap angle given by the expression

$$\theta_{pc} = \sin^{-1} \left(\frac{2\pi R}{cP} \right)^{1/2}, \quad (12)$$

where P is the pulsar period in seconds, R is the neutron star radius (10^6 cm) and c is the speed of light. We partition the open field lines through a dimensionless parameter, ξ , that varies between 0 and 1 and is defined as

$$\xi = \frac{\theta_s}{\theta_{pc}}, \quad (13)$$

where θ_s is the polar angle of the open field line at the intersection with the surface of the star. The particle emits curvature photons along the line of sight at an angle $\theta_\gamma = 3\theta/2$ given by

$$\cos \theta_\gamma = \sin \alpha \sin \zeta \cos \phi + \cos \alpha \cos \zeta, \quad (14)$$

where ϕ is the phase angle, α is the magnetic inclination and ζ is the viewing angle.

We approximate the accelerating electric field from Equation 14 of Harding & Muslimov (1998) using the expression

$$E_{||} = \sin^4(\theta_{pc}) B_{12} \left[\kappa \cos \alpha \eta^{-4} + \frac{1}{8} \sin^{1/2}(\theta_{pc}) \xi \sin \alpha \cos \varphi \eta^{-1/2} \right] (1 - \xi^2) \text{ statvolt} \cdot \text{cm}^{-1}, \quad (15)$$

where $\kappa = 0.15$ is the general relativistic inertial frame dragging factor, B_{12} is the surface magnetic field in units of 10^{12} G, $\eta = r/R$ is the dimensionless radius and φ is the azimuth angle around the magnetic pole given by the expression

$$\cos \varphi = \frac{\cos \zeta - \cos \alpha \cos \theta_\gamma}{\sin \alpha \sin \theta_\gamma}. \quad (16)$$

The gain in energy of the accelerating primary electron is compensated by the CR losses (Harding, Muslimov & Zhang 2002; Bulik, Rudak & Dyks 2000; Lou, Shibata, & Melrose 2000), so that the electron Lorentz factor γ becomes radiation-reaction limited to

$$e |E_{||}| \sim \frac{2e^2 \gamma^4}{3\rho_c^2}, \quad (17)$$

where ρ_c is the classical radius of curvature of the field line given by

$$\rho_c = \frac{r (1 + \cos^2 \theta)^{3/2}}{3 \sin \theta (1 + \cos \theta)}. \quad (18)$$

At low altitudes near the stellar surface, $r < R(\sin \theta_{pc}/3 + 1)$, the near surface electric field is approximated from equation 21 in Harding & Muslimov (2001) by the expression

$$E_{\parallel} = -4.05B_{12} \sin^3 \theta_{pc}(\eta-1) \left[0.15(1 - \xi^{2.19})^{0.705} \cos \alpha + \frac{3}{8} \sin \theta_{pc} \xi^{1.015} (1 - \xi^2)^{0.65} \sin \alpha \cos \varphi \right] \quad (19)$$

and goes to zero at the stellar surface. The CR spectrum therefore has a spectral index of $-2/3$ with a high-energy cutoff ϵ_{CR} given by

$$\epsilon_{CR} = \left(\frac{3\lambda_C \gamma^3}{2\rho_c} \right) = \hbar c \left(\frac{3}{2} \right)^{7/4} \left(\frac{E_{\parallel}}{e} \right)^{3/4} \rho_c^{1/2}, \quad (20)$$

in $m_e c^2$ units where e is the electron charge and $\lambda_C \equiv \hbar/(m_e c)$ is the electron Compton wavelength.

The instantaneous curvature radiation power spectrum has the form (Jackson 1975)

$$P_{CR}(\epsilon_{\gamma}, \theta_{\gamma}, \xi) = 3^{1/2} \alpha_{\text{fine}} \gamma \left(\frac{c}{2\pi\rho_c} \right) \kappa \left(\frac{\epsilon_{\gamma}}{\epsilon_{CR}} \right), \quad (21)$$

where ϵ is the photon energy, γ is the particle Lorentz factor, α_{fine} is the fine structure constant, and the $\kappa(x)$ function is defined as

$$\kappa(x) = x \int_x^{\infty} K_{5/3}(x') dx' \approx \begin{cases} 2^{2/3} \Gamma\left(\frac{2}{3}\right) x^{1/3}, & x \ll 1, \\ 1.253 x^{1/2} e^{-x}, & x \gg 1 \end{cases} \quad (22)$$

We find that the low energy asymptotic form provides a sufficiently accurate description of the power spectrum above $\epsilon_{\gamma}=100$ MeV and the instantaneous curvature photon radiation spectrum per primary is given by

$$N_{CR}(\epsilon, \theta_{\gamma}, \xi, \varphi) = \frac{3^{1/6} \Gamma\left(\frac{2}{3}\right) \alpha_{\text{fine}}}{\pi \hbar^{1/3}} \left(\frac{c}{\rho_c} \right)^{2/3} \epsilon^{-2/3} \sim \frac{0.518 \alpha_{\text{fine}}}{\hbar^{1/3}} \left(\frac{c}{\rho_c} \right)^{2/3} \epsilon^{-2/3}, \quad (23)$$

which is similar to equation 7 in Harding, Usov, & Muslimov (2005). This expression can be integrated from $\epsilon_{\gamma}=100$ MeV to the high-energy cut off ϵ_{CR} to give the expression

$$N_{CR>(> \epsilon_{\gamma}, \theta_{\gamma}, \xi, \varphi) = \frac{1.554 \alpha_{\text{fine}}}{\hbar^{1/3}} \left(\frac{c}{\rho_c} \right)^{2/3} \left(\epsilon_{\gamma}^{1/3} - \epsilon_{CR}^{1/3} \right), \quad (24)$$

which provides the number of curvature photons emitted along the line of sight θ_{γ} from an open field line ξ at a radial distance r per primary particle, where r is given by the expression

$$r = \frac{R \sin^2 \theta}{\sin^2(\xi \theta_{pc})}. \quad (25)$$

The Goldreich-Julian current of primary particles from the polar cap is uniformly distributed over the polar cap and is given by the expression

$$\dot{N}_p = 1.3 \times 10^{30} B_{12} P^{-2} \text{ particles/s.} \quad (26)$$

The number of primary particles in a particular patch on the stellar surface at R , θ_s , and φ , which gives the number of primaries along a particular field line ξ , is provided by the expression

$$\dot{n}_{GJ} = \frac{\dot{N}_{GJ}}{2\pi(1 - \cos \theta_{pc})}. \quad (27)$$

The total photon luminosity from one pole can be obtained by integrating over the open field volume to give

$$L_{\text{total}}(> \varepsilon_\gamma) = \dot{n}_{GJ} \int_0^{2\pi} \int_0^1 \int_R^{R_{LC}} N_{CR}(> \varepsilon_\gamma, \theta_\gamma, \xi, \varphi) \theta_{pc} \sin \xi \theta_{pc} dr d\xi d\varphi. \quad (28)$$

With

$$\left(\frac{dr}{d\theta} \right) = \frac{2R \sin \theta \cos \theta}{\sin^2(\xi \theta_{pc})}, \quad (29)$$

the integral over r can be written as an integral over θ to give

$$L_{\text{total}}(> \varepsilon_\gamma) = \int_0^{2\pi} \int_0^1 \int_{\theta(R)}^{\theta(R_{LC})} \left(\frac{2R \dot{n}_{GJ} N_{CR}(> \varepsilon_\gamma, \theta_\gamma, \xi, \varphi) \theta_{pc} \cos \theta}{c \sin(\xi \theta_{pc})} \right) \sin \theta d\theta d\xi d\varphi. \quad (30)$$

where the integral over ξ (the θ_{pc} has been included in the integrand) is over the open field lines and $\xi \theta_{pc}$ is the angle at the footpoint of the field line on the stellar surface. The expression in parentheses represents the photon emission from a particular field line at ξ and η , integrated above $\varepsilon_\gamma=100$ MeV, along the line of sight into a solid angle $d\Omega$ and is given by the expression

$$\frac{dN_{CR}(> \varepsilon_\gamma, \theta_\gamma, \xi, \varphi)}{d\Omega} = \frac{1.552 \alpha_{fine} \dot{N}_{GJ} c R \theta_{pc} \rho_c^{-2/3} \cos \theta \left(\varepsilon_\gamma^{1/3} - \varepsilon_{CR}^{1/3} \right)}{\pi(1 - \cos \theta_{pc})(\hbar c)^{1/3} \sin(\xi \theta_{pc})}. \quad (31)$$

The total emission from the polar cap for a particular phase bin ϕ is obtained by integrating over parameter ξ to include the contributions of all the open field lines along a line of sight defined by the viewing angle ζ . The total emission in the phase bin is given by

$$N_{CR}^{\text{tot}}(> \varepsilon_\gamma, \phi) = \int_0^1 \frac{dN_{CR}(> \varepsilon_\gamma, \theta_\gamma, \xi, \varphi)}{d\Omega} d\xi, \quad (32)$$

Having calculated the γ -ray pulse profile for each MSP for a given viewing geometry, we average the profile to obtain the average photon flux, and compare it to the instrument threshold. Our resulting γ -ray efficiency (7%) for the total spectrum and profiles for the nearby MSP PSR J0437+4715 are in agreement with those obtained by Venter & DeJager (2005).

8. Gamma-ray All Sky Threshold Maps

From the simulated γ -ray pulse profile, we obtain an average flux that we compare to all sky threshold maps for EGRET, AGILE and GLAST Large Area Telescope (LAT). We use the recently revised EGRET map that includes the dark clouds (Casandjian & Grenier 2007), which has led to a radical reassessment of the EGRET unidentified sources. The GLAST threshold has been improved and updated (Grenier & Casandjian private communication) as a 1 year GLAST LAT threshold map. The all sky map for AGILE (Pellizzoni private communication) has not been recently updated in our computer code. The detection of radio and γ -ray point sources within the code are independent of each other, allowing the tagging of radio-quiet (below the survey flux thresholds) and radio-loud γ -ray MSPs.

9. Results

To improve the simulated statistics, we run the simulation to obtain ten times the number of detected MSPs and then normalize the distributions accordingly. In Figure 4, we present Aitoff projections for the detected (a) and simulated (b) MSPs. Since MSPs are closer to us and are much older than NPs, the graphs indicate larger out-of-plane distributions than those of NPs.

Of the ten radio surveys that we have included in our simulation, the surveys most sensitive to MSP detection are Parkes 2, Parkes Multibeam and Swinburne Intermediate Latitude which together account for majority of the 56 MSPs, as seen in Table 1. Within the limited statistics, there is good agreement between the number of MSPs detected and simulated among the ten surveys used in our selected group. The few detections in radio surveys that are not very sensitive to the detection of MSPs are also well reproduced by the simulation.

The distributions in the $\dot{P} - P$ diagram are compared in Figure 5 for detected (a) and simulated (b) MSPs. The dotted broken lines represent the pair death lines for curvature radiation (CR) and for nonresonant inverse Compton scattering (NRICS). Below the CR death line, CR no longer is able to produce pairs. However, a limited number of pairs can still be produced via inverse Compton scattering above the NRICS death line. Below the NRICS death line, pair production is no longer possible, presumably inhibiting radio emission mechanisms. The upper and lower MSP birth lines indicated by the solid lines represent the approximate Eddington critical accretion rate (upper line) and 5×10^{-4} times that rate (lower line) discussed earlier. With the $B^{-3/2}$ magnetic field distribution and the uniform distribution of birth lines between the upper and lower MSP birth lines, we reproduce the

observed broadness of the pulsar distribution in the $\dot{P} - P$ diagram.

In Figure 6, we present histograms of the indicated measured and derived pulsar characteristics for the detected (shaded histograms), and the simulated (unshaded histograms) MSPs. Although the poor statistics make it difficult to judge the agreement, the simulation appears to reproduce the observed distributions fairly well. The clump of detected MSPs observed in Figure 5a is exhibited as narrow peaks in the period and period derivative distributions. The narrow peak in the period derivative distribution is not present in the simulated distribution. In the comparisons of the age distributions, we calculated the traditional characteristic age $P/(2\dot{P})$ for the simulated pulsars. In the comparisons of the distances and dispersion measures of the MSPs, we have used the new distance model of Cordes & Lazio (2002). The distance of the detected pulsar is established typically by its measured dispersion measure and location in the sky. The new distance model is used to determine the simulated dispersion measure from the simulated distance and location in the sky for each MSPs, which is then used in the calculation of the flux threshold S_{min} for each radio survey. Both the simulated dispersion measure and distance distributions indicate good agreement with the corresponding distributions of detected MSPs with a few more simulated closer pulsars. The simulated radial and height distributions within the Galaxy are consistent with those distributions of the detected pulsars. However, the simulated spectral index distribution is narrower than that of the detected pulsars. For the pulsar characteristics in Figure 6, we have performed a Kolmogorov-Smirnov (KS) statistics test of the histograms assuming a significance level (α) of 5%. We indicate in Figure 6 the resulting p-values for each of the comparisons. Sometimes the D statistic and the critical value are quoted in the literature and compared to each other to decide on the null hypothesis. The critical value is derived from α and the number of samples. Equivalent comparisons can be made between the p-value and α . If the p-value statistic is larger than α , the null hypothesis is not excluded at the level of significance determined by α . Our results indicate that in all comparisons, the distributions of simulated pulsars are consistent with those detected with the exception of the distributions of the Galactic height z and S400 whose p-value is less than 0.005. In the case of the S400 distributions, the statistics are insufficient in the number of measured flux densities at 400 MHz for an adequate comparison. We simulate slightly more pulsars with larger S1400 fluxes. We applied the two dimensional KS test to the unbinned period and period derivative distributions using the prescription of Press et al. (2002) and obtained a p-value of only of 0.03 at the same significance level of 5% indicating that the detected and simulated $\dot{P} - P$ distributions are not entirely consistent with each other. While the KS tests might be helpful in such comparisons, the numerous assumptions within the simulation, such as the radio luminosity, the pulsar distance, and birth distributions, contain systematic uncertainties. Therefore, we do not want to overemphasize the importance of

these statistical tests.

The detection of a radio pulsar in the computer code is independent of the detection of a γ -ray pulsar, allowing the identification of radio-quiet and radio-loud γ -ray pulsars. By radio-quiet, we mean that the radio flux of the simulated pulsars is below the flux threshold of the surveys that could potentially observe it; otherwise, the pulsar is flagged as radio-loud. In Figure 7, we show the simulated radio-quiet and radio-loud γ -ray MSPs for the instruments EGRET (upper right), AGILE (lower left) and GLAST LAT (lower right). For comparison, we also show the γ -ray pulsars that were detected by EGRET (upper left), including the MSP J0218+4232. In the case of Geminga (cross in upper right), it is not clear whether its radio silence results from a misalignment of the γ -ray and radio beams or from its intrinsic radio weakness. While it is unclear how many of the EGRET unidentified sources might be MSPs detected as point sources, the simulation predicts that a few may be radio-quiet γ -ray MSPs.

All the simulated γ -ray pulsars that are detected by EGRET, AGILE and GLAST lie below the curvature radiation pair death line in the $\dot{P} - P$ diagram (Figure 7). As discussed above, in this pair-starved polar cap model, curvature radiation escapes along all open field lines. However, as indicated by Harding, Usov, & Muslimov (2005), curvature radiation can be limited when the accelerated particles undergo resonant cyclotron absorption of radio photons under special circumstances. The excited particles emit synchrotron radiation typically at lower energies than curvature radiation. While we are in the process of developing a full three-dimensional study of these processes, in the present calculation we have not limited the curvature radiation in altitude. Therefore, our results may be somewhat optimistic. In Figure 7, the γ -ray MSPs cluster in the lower left of the $\dot{P} - P$ diagram because the γ -ray luminosity increases with decreasing P .

In Table 2, we present the γ -ray MSPs statistics for radio-loud and radio-quiet pulsars. Due to the uncertainties in the radio luminosity, we vary the coefficient of the radio luminosity in Equation 8 by $\pm 10\%$ to obtain a range in radio-quiet γ -ray pulsars. Since the simulation is normalized to the detected number of radio pulsars, there is no variation in the number of radio-loud γ -ray pulsars. Of the 33-40 radio-quiet γ -ray MSPs predicted to be detected by GLAST, about 6 have fluxes above the 10^{-7} photons/cm²/s level (Grenier, private communication), that GLAST may be able to detect through blind period searches. However, since 70% of the MSPs in the ATNF catalogue are in binaries, many of these radio-quiet γ -ray pulsars are expected to be in binary systems. It will be difficult for GLAST to detect pulsed emission from these MSPs in blind period searches due to timing uncertainties associated with the orbital motion. Without radio ephemerides, GLAST will detect binary MSPs only as point sources.

In order to explore the nature of the radio-quietness of the GLAST pulsars, we present in Figure 8 histograms of the radio flux at 1400 MHz of the detected (solid dark gray histograms) and simulated (open thin histograms) radio pulsars in (a) and the radio flux of GLAST radio-quiet (solid light gray histograms) and radio-loud (open thick histograms) in (b). As expected, GLAST radio-loud pulsars have large radio fluxes. However, the GLAST radio-quiet pulsars form two groups, one with a flux distribution very similar to the radio detected and simulated pulsars in Figure 8a and the other with a much lower flux distribution that would be difficult to detect without deep radio pointings.

The Parkes Multibeam and Swinburne Intermediate Latitude surveys are the two most sensitive surveys in our select group of radio surveys. However, they cover a rather narrow strip along the Galactic disk, and MSPs seem to be rather scattered in space and are not as correlated with the Galactic disk as are NPs. As a result, many of the GLAST detected pulsars are radio-quiet because they happen to be outside the sensitive survey regions or have radio fluxes that are slightly lower than the survey thresholds.

In Figure 9, we plot the impact angle $\beta = \zeta - \alpha$ as a function of the radio flux at 1400 MHz for the simulated group of GLAST radio-quiet pulsars. We can see that the two groups of fluxes correspond to two groups of impact angles. The MSPs in the low flux group with large impact angles will not be observed as radio sources without deep radio observations. However, the simulation suggests that they can be seen as γ -ray point sources. In the pair-starved model of γ -ray emission, curvature radiation occurs along all open field lines all the way out to the light cylinder. While the intensity of curvature radiation decreases at higher altitudes for nearby pulsars, we predict that GLAST should be able to detect them as point sources, yet their radio emission will be very difficult to detect as the radio beam and the γ -ray beam are separated by large angles. However, the higher flux group with smaller impact angles would be detected by GLAST as point sources and potentially are detectable with pointed radio observations.

As a result, our simulations suggest that it will be important to follow up GLAST detections with radio observations in order to discover a greater number of radio-loud γ -ray pulsars. The predicted energy spectra of MSPs are very different than those of either NPs or AGNs. In this pair-starved polar cap model, the energy cutoffs of the MSP γ -ray spectra are predicted to be in the 10-50 GeV energy region (Harding, Usov, & Muslimov 2005) suitable for GLAST.

Clearly the number of detected radio-quiet and radio-loud γ -ray MSPs depends strongly on the detection thresholds of radio surveys and γ -ray instruments. In Figure 10, we present the Log(N)-Log(S) for the radio flux at 400 MHz (a) and 1400 MHz (b) and for EGRET (c) and GLAST (d). The light shaded histograms represent the simulated undetected source

counts. The dark histograms represent the simulated detected source counts by the select group of ten radio surveys at 400 MHz (a) and 1400 MHz (b). For EGRET (c) and GLAST (d), the dark and medium dark histograms represent the simulated source counts for radio-loud and radio-quiet γ -ray MSPs, respectively.

The appearance of fractions of a pulsar in the figure is a result of the re-normalizing the distributions because the simulation was run for ten times the number of detected MSPs to improve the simulated statistics. Assuming a uniform distribution of sources in space with isotropic emission of equal flux, one expects to a slope in the Log(N)-Log(S) diagram of $-3/2$. Indeed the tails of these distributions have slopes very similar to $-3/2$. While for EGRET and GLAST the Log(N)s of simulated detections have a sharp decrease with decreasing flux, the Log(N)s of simulated radio detections have a more gentle roll over, which may reflect the larger number of factors that determine the minimum flux threshold for the radio surveys. Both the number of undetected radio and γ -ray sources follow a simple power law far below the sensitivity of the radio surveys and γ -ray instruments.

10. Discussion

We have presented a Monte-Carlo simulation of the Galactic-plane population of MSPs and corresponding predictions for the numbers of both radio-quiet and radio-loud MSPs that are detectable as γ -ray sources. In order to accomplish this, we made significant improvements in our population statistics Monte Carlo code by adding the more realistic description of the Galactic potential of Dehnen & Binney (1998) with a more accurate 5th order Cash-Karp Runge-Kutta trajectory integration routine (Press et al. 1992), using improved all-sky threshold maps for EGRET (Casandjian & Grenier 2007) and GLAST (Grenier & Casandjian, private communication), and including the Swinburne Intermediate Latitude radio survey (Edwards et al. 2001). We have modified the intrinsic radio luminosity model of ACC to describe the total radio luminosity of both normal and MSPs. From our study of radio pulsars with three-peak profiles (Gonthier et al. 2006, 2007), we find that the ratio of the core-to-cone peak fluxes for short period pulsars is much smaller for short period pulsars than the ratio predicted by ACC model. Although MSPs have on average larger pulse widths than NPs, this resulting radio beam geometry model provides a reasonable agreement to the average pseudoluminities and pulse widths at 1400 MHz and pulse widths of both NPs and MSPs. We include a γ -ray beam geometry and luminosity model of the curvature radiation from all open field lines within a pair-starved polar cap model (Harding, Usov, & Muslimov 2005) that accounts for γ -ray emission below the curvature radiation pair death line, which is applicable to MSPs. These improvements in our computer code have allowed us to study

the population statistics of radio and γ -ray MSPs to complement our previous studies of NPs from the Galactic disk. As a first order study, we believe that we have improved the simulation by including a beam geometry for MSPs and an intrinsic radio luminosity whose functional form allows for the description of the population statistics of normal pulsars. The actual beam geometry of MSPs may turn out to be significantly different and require a different model than the one proposed here from the work of Kijak & Gil (1998, 2003). The population statistics study is not sensitive enough to discriminate between beam geometry models as the average flux of the profile is the quantity that is compared to the S_{mins} of the radio surveys. A detailed study including relativistic effects will be necessary along with high quality polarization data may enable establishment of systematic trends that allows for the development of an adequate beam model for MSPs.

In this study, we do not attempt to describe the numerous MSPs within globular clusters. Limiting our study to the MSPs born in the Galactic disk, we treat them as point particles, evolving their location within the Galactic potential and their spin-down, after spin-up by mass accretion from a binary companion star has ended. This group of old, short period pulsars with low magnetic fields are given radio and γ -ray beam and luminosity characteristics and filtered through a set of ten radio surveys and the γ -ray instruments EGRET, AGILE and GLAST. Our simulation is run until the number of simulated radio pulsars is equal to the number detected by the same group of radio surveys. The radio luminosity is adjusted in our study of NPs (Gonthier et al. 2007; Harding, Grenier & Gonthier 2006) to give a birth rate of Type II supernovae of 2.1 per century to agree with the study of Tammann, Löffler & Schröder (1994) and to reproduce the detected mean pseudoluminities and spectral indices of MSPs and NPs, after which there are no further adjustments performed in the simulation of MSPs. Allowing for a $\pm 10\%$ variation in the radio luminosity, we predict a birth rate of $4-5 \times 10^{-4}$ MSPs per century, which is in good agreement with the studies of Lorimer (2005) (3×10^{-4} per century) and Ferrario & Wickramasinghe (2006) (3.2×10^{-4} per century). While the population statistics studies of LMXBs contain numerous uncertainties, our simulated birth rate agrees with the estimate of the birth rate of LMXBs from the preferred model (F) of Kiel & Hurley (2006) (6.5×10^{-4} per century). We are also in agreement with Kramer et al. (1998) as our description of the spectral properties of the core and cone beams for MSPs requires steeper angle-integrated spectral indices than those for the simulated NPs.

In outer gap accelerator models (Cheng, Ho & Ruderman 1986), MSPs are not expected to produce γ -ray emission above 1-2 GeV (Zhang & Cheng (2003), Hirotani private communication 2005) due to the smaller electric field and larger radius of curvature in the gap. Thus, detected emission from MSPs above 5 GeV would imply an origin near the polar cap. Zhang & Cheng (2003) propose that particles accelerated in the outer gaps could be

the origin of MSP radiation at super-GeV energies, but only if the cascade emission from the particles as they travel down toward the neutron star surface is visible. However, it seems unlikely that both the upward-going radio emission and downward-going γ -ray emission could be visible to the same observer. In that event, one would expect the radio and high-energy peaks to be out of phase, and X-ray and radio peaks are often in phase for MSPs (e.g. B1821-24, J0437-4715, B1921+37). In any case, GLAST observations of MSPs will be an excellent model discriminator.

Our simulations predict the number of radio-loud and radio-quiet γ -ray pulsars observed by the instruments EGRET, AGILE and GLAST. EGRET was only able to detect one MSP, PSR J0218+4232, during its nine-year mission. EGRET did not have the capability of performing blind period searches of pulsars and required reliable radio ephemerides to detect γ -ray pulsations. However, these observations were prior to the Parkes Multibeam Pulsar Survey and the Swinburne Intermediate Latitude Survey that tripled the number of detected radio MSPs in Galaxy (not counting those in globular clusters). We predict that EGRET should have detected as point sources eight radio-loud and ~ 20 radio-quiet γ -ray MSPs, some of which could be associated with EGRET unidentified sources. However, the recently revised all-sky EGRET threshold map with dark clouds (Casandjian & Grenier 2007), used in our simulations, has significantly affected the catalogue of EGRET unidentified sources. As the all-sky threshold map for AGILE has not been recently updated, our predictions for AGILE might be somewhat optimistic. However, the trend in the statistics for EGRET, AGILE and GLAST suggests that the number of radio-quiet and radio-loud γ -ray MSPs predicted to be detected by AGILE might be reasonable. The Shklovskii effect is a significant, positive contribution to the intrinsic \dot{P} of the pulsar resulting in much larger measured \dot{P} s and needs to be taken into account in population statistics studies. The effect of having to decrease the intrinsic \dot{P} to accommodate this effect results in pulsars with lower γ -ray luminosities. We predict ~ 38 of radio-quiet γ -ray pulsars for GLAST with the ratio of radio-quiet to radio-loud increasing from 1.5 for EGRET to 3.2 for GLAST. Curvature radiation of γ -rays below the curvature pair death line occurs along all open field lines all the way out to the light cylinder, as the weak production of pairs through nonresonant inverse Compton scattering is insufficient to screen the electric field. The increased sensitivity of GLAST results in a large number of detections at higher altitudes where the γ -ray beam is at large angles relative to the radio beam, resulting in radio fluxes below the flux thresholds of our select group of radio surveys. However, in many cases, the radio fluxes are relatively large but are outside of the sky region of the Parkes Multibeam and Swinburne Intermediate Latitude surveys. MSPs are much less confined to the plane of the Galactic disk than are NPs and therefore often appear at high latitudes, far above the narrow belt covered by these more sensitive surveys. Our simulations suggest that GLAST will detect many MSPs as

point sources, and only a handful as radio-loud pulsars. The point sources can be identified as pulsar candidates by their spectra. Harding, Usov, & Muslimov (2005) indicate that the curvature radiation energy spectra of MSPs are very hard, with cutoffs in the region of 10 to 50 GeV, well within the GLAST range. Such detected candidates can easily be followed up with pointed radio observations to obtain the periods of the pulsars. Thus, GLAST with radio follow-up observations offers the potential to discover many new MSPs in the Galaxy.

We are very grateful to Isabelle Grenier and Jean-Marc Casandjian for providing a GLAST-LAT 1 year point source threshold map. We express our appreciation to the anonymous referee for the insightful comments, which led to a much-improved manuscript. We are indebted to Dunc Lorimer who pointed out our neglect of the Shklovskii effect in an earlier version of the manuscript. We express our gratitude for the generous support of the National Science Foundation (REU and AST-0307365), the Michigan Space Grant Consortium and the NASA Astrophysics Theory Program.

REFERENCES

- Alpar, M.A., Cheng, A.F., Ruderman, M.A., & Shaham, J. 1982, *Nature*, 300, 728
- Arzoumanian, Z., Chernoff, D.F., & Cordes, J.M. 2002, *ApJ*, 568, 289
- Bailes et al. 1997, *ApJ*, 481, 386
- Bhattacharya, D. & van den Heuvel, E.P.J. 1991, *Phys. Rev.*, 203, 1
- Bulik, T., Rudak, B. & Dyks, J. 2000, *MNRAS*, 317, 97
- Camilo, F., Thorsett, S., & Kulkarni, S.R. 1994, *ApJ*, 421, L15
- Casandjian, J. & Grenier, I.A. 2007, *Ap&SS*, in press
- Chakrabarty, D. in *Accretion, Evolution, and Outcomes*. AIP Conference Proceedings, Volume 797, pp. 71-80 (2005)
- Cheng, K. S., Ho, C. & Ruderman, M. A. 1986, *ApJ*, 300, 500
- Cordes, J.M., & Chernoff, D.F. 1997, *ApJ*, 482, 971
- Cordes, J.M. & Lazio, T.J.W. 2002, astro-ph/0207156
- Crawford, F. Manchester, R.N. & Kaspi, V.M., 2001, *AJ*, 122, 2001

- Crawford, F. & Keim, N.C. 2003, *ApJ*, 590, 1020
- Dehnen, W. & Binney, J. 1998, *MNRAS*, 294, 429
- Dyks, J., & Harding A.K., 2004, *ApJ*, 614, 869
- Dyks, J., Harding, A.K., & Rudak, B. 2004, *ApJ*, 606, 1125
- Dyks, J. & Rudak, B. 2003, *ApJ*, 598, 1201
- Edwards, R. T. et al. 2005, *MNRAS*, 326, 358
- Faucher-Giguère, C. & Kaspi, V. M. 2006, *ApJ*, 643, 332
- Faulkner et al. 2005, *ApJ*, 618, L119
- Faulkner et al. 2004, *MNRAS*, 355, 147
- Ferrario, L. & Wickramasinghe, D. 2006, *MNRAS*, 375, 1009
- Gonthier, P.L., Ouellette, M.S., Berrier, J., O'Brien, S., & Harding, A.K. 2002, *ApJ*, 565, 482
- Gonthier, P.L., Van Guilder, R. & Harding, A.K. 2004, *ApJ*, 604, 775
- Gonthier et al. 2006, *Chin. J. Astron. Astrophys.*, 6, 97
- Gonthier, P.L., Story, S.A., Clow, B.D., & Harding, A.K. 2007, *Ap&SS*, in press, astro-ph/0702097
- Grimm, H.-J., Gilganov, M., & Sunyaev, R. 2002, *A&A*, 391, 923
- Harding, A.K. & Muslimov, A.G. 1998, *ApJ*, 508, 328
- Harding, A.K., Muslimov, A.G., & Zhang, B. 2002, *ApJ*, 576, 366
- Harding, A.K. & Muslimov, A. 2001, *ApJ*, 556, 987
- Harding, A.K., Greiner, I.A. & Gonthier, P.L. 2006, *Ap&SS*, in press, astro-ph/0703019
- Harding, A.K., Usov, V.V., & Muslimov, A. 2005, *ApJ*, 622, 531
- Hobbs et al. 2004, *MNRAS*, 352, 1439
- Hobbs et al. 2005, *MNRAS*, 360, 963
- Jackson, J.D. 1975, *Classical Electrodynamics* (New York: Wiley)

- Jiang, Z.J. & Zhang, L., 2006, ApJ, 643, 1130
- Johnston, S. & Weisberg, J.M. 2006, MNRAS, 368, 1856
- Kiel, P. D. & Hurley, J. R. 2006, MNRAS, 369, 1152
- Kijak, J., & Gil, J. 1998, MNRAS, 299, 855
- Kijak, J., & Gil, J. 2003, A&A, 397, 969
- Kramer, M. et al. 1997, A&A, 322, 846
- Kramer, M. et al. 1998, ApJ, 501, 270
- Kramer, M. et al. 1999, ApJ, 526, 957
- Kramer, M. 2002, in Neutron Stars, Pulsars and Supernova Remnants, Proceedings of the 270. WE-Heraeus Seminar held in Bad Honned, Germany, Ed. by W. Becker, H. Lesch, & J. Trümper, 278, 177
- Kramer et al. 2003, MNRAS, 342, 1299
- Krolik, J. 1991, ApJ, 373, L69
- Kuiper, L., Hermsen, W., & Stappers, B. 2003, in Pulsars, AXPs and SGRs Observed with BeppoSAX and Other Observatories, Proceedings of the International Workshop held in Marsala, Ed. by G. Cusumano, E. Massaro, & T. Mineo, 31
- Lamb, F.K., & Yu W., In Proc. ASP Conference Series, *Binary Radio Pulsars*, Ed. By F.A. Rasio & I.H. Stairs, 2005, 328, 299
- Lommen et al. 2000, ApJ, 545, 1007
- Lorimer, D.R. Yates, J.A., Lyne, A.G. & Gould, D.M. 1995, MNRAS, 273, 411
- Lorimer, D. 2005, Living Rev. Rel. 8, 7
- Lorimer et al. 2006, MNRAS, 372, 777
- Lou, Q., Shibata, S. & Melrose, D. B. 2000, MNRAS, 318, 943
- Manchester, R. N. 1996, in IAU Colloq. 160, *Pulsars: Problems and Progress*, ed. S. Johnston, M. Bailes, & M. Walker (ASP Conf. Ser. 105; San Francisco: ASP), 193

- Manchester, R.N. 1999 in *Pulsar Timing, General Relativity and the Internal Structure of Neutron Stars*, Edited by Z. Arzoumanian, F. Van der Hooft, and E. P. J. van den Heuvel. Koninklijke Nederlandse Akademie van Wetenschappen, Amsterdam, The Netherlands, ISBN 90-6984-247-5, 53
- Manchester et al. 2001, *MNRAS*, 328, 17
- Manchester, R. N., Hobbs, G. B., Teoh, A. & Hobbs, M. 2005 *AJ*, 129, 1993
- Mitra, D. & Deshpande, A. A. 1999, *A&A*, 346, 906
- Morris et al. 2002, *MNRAS*, 335, 275
- Muslimov, A.G. & Harding, A.K. 2004, *ApJ*, 606, 1143
- Muslimov, A.G. & Harding, A.K. 2003, *ApJ*, 588, 430
- Paczyński, B. 1990, *ApJ*, 348, 485
- Press, W.H. et al. 1992, *Numerical Recipes in C The Art of Scientific Computing*, Cambridge University Press New York
- Press, W.H. et al. 1992, *Numerical Recipes in C & C++ Source Code v 2.11*, Cambridge University Press New York
- Shklovskii, I.S., 1970, *Soviet Astronomy*, 13, 562
- Story, S.A., Gonthier, P.L., Clow, B.D., & Harding, A.K., 2006, *AAS*, 209, #159.07
- Stairs et al. 2005, *ApJ*, 632, 1060
- Tammann, G. A., Löffler, W., & Schröder, A. 1994, *ApJS*, 92, 487
- Thompson, D.J. in *Cosmic Gamma-ray Sources*, ed. K.S. Cheng & G.E. Romero, (Kluwer) p. 149 (2004)
- Toscano, M. Bailes, M. Manchester, R., & Sandhu, J. 1998, *ApJ*, 506, 863
- Toscano, M. et al. 1999, *MNRAS*, 307, 925
- Venter, C. & DeJager, O. C. 2005, *ApJ*, 619, L167
- Vranesevic et al. 2004, *ApJ*, 617, L139
- Wang, W., Jiang, Z. J., & Cheng, K. S. 2005, *MNRAS*, 358, 263

Xilouris, K.M. et al. 1998, ApJ, 501, 286

Zhang, L. & Cheng, K. S. 2003, A&A, 398, 639

Table 1: Detected and Simulated MSPs in each Radio Survey

Survey	Frequency (MHz)	Detected	Simulated
Arecibo 3	430	4	8
Arecibo 2	430	2	1
Greenbank 3	390	0	3
Greenbank 2	390	1	0
Molongo 2	408	0	1
Parkes 2	436	18	23
Parkes 1	1520	0	0
Jodrell Bank 2	1400	0	0
Parkes MB	1374	28	20
Swinburne IL	1374	12	9

Table 2: Simulated γ -ray MSP statistics

Instrument	Radio-loud	Radio-quiet	Ratio RQ/RL
EGRET detected	1	?	
EGRET simulated	4	5 - 6	1.5
AGILE simulated	7	11 - 13	1.9
GLAST simulated	12	33 - 40	3.2

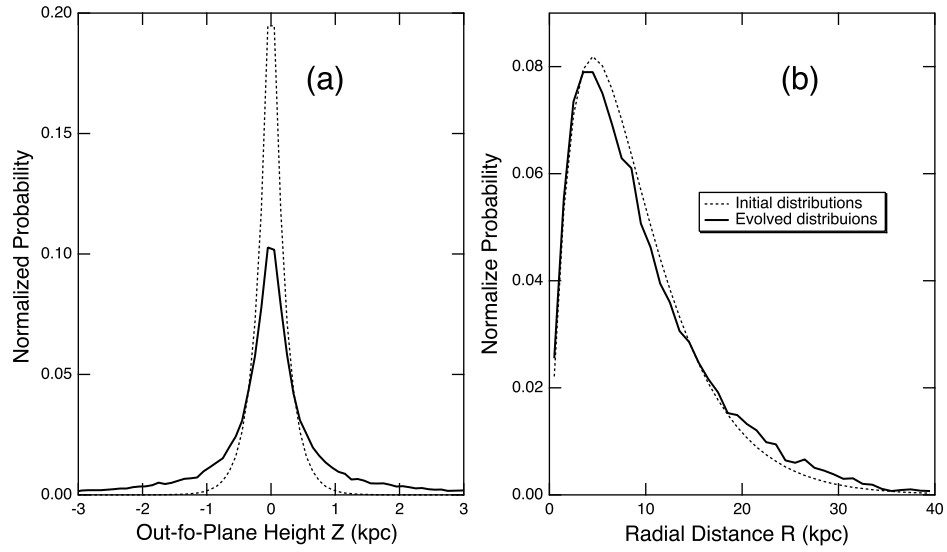


Fig. 1.— Height above the Galactic plane Z (a) and Galactic radius R (b) distributions of millisecond pulsars. Initial distributions are indicated by dotted curves and equilibrium distributions by solid curves.

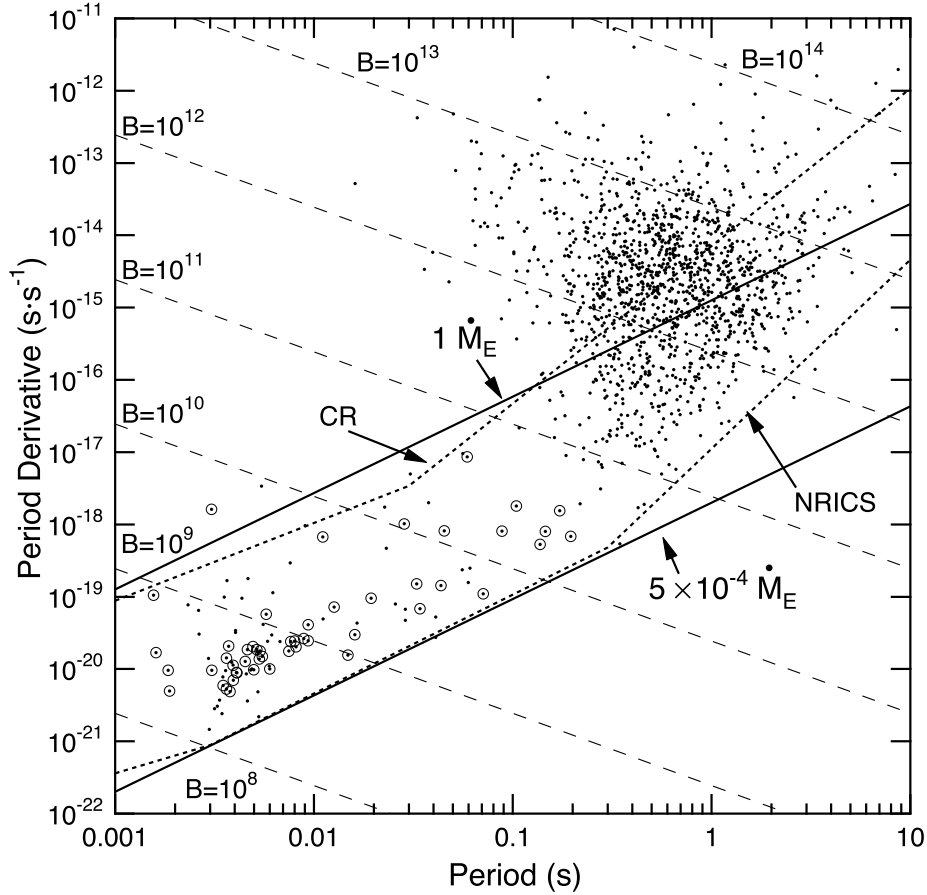


Fig. 2.— $\dot{P} - P$ diagram of radio pulsars (dots) in the ATNF catalogue (<http://www.atnf.csiro.au/people/pulsar/psrcat/> and Manchester et al. (2005)). Millisecond pulsars detected by the group of ten radio surveys used in this study are indicated with an additional open circle. The thin dashed lines represent the indicated traditional magnetic surface strength, assuming a constant dipole spin-down field. The dotted broken lines represent the pair death lines for curvature radiation (CR) and for nonresonant inverse Compton scattering (NRICS). The upper and lower MSPs birth lines for Eddington critical accretion rate \dot{M}_E (above) and $5 \times 10^{-4} \dot{M}_E$ of that rate (below) discussed in the text are indicated by solid lines.

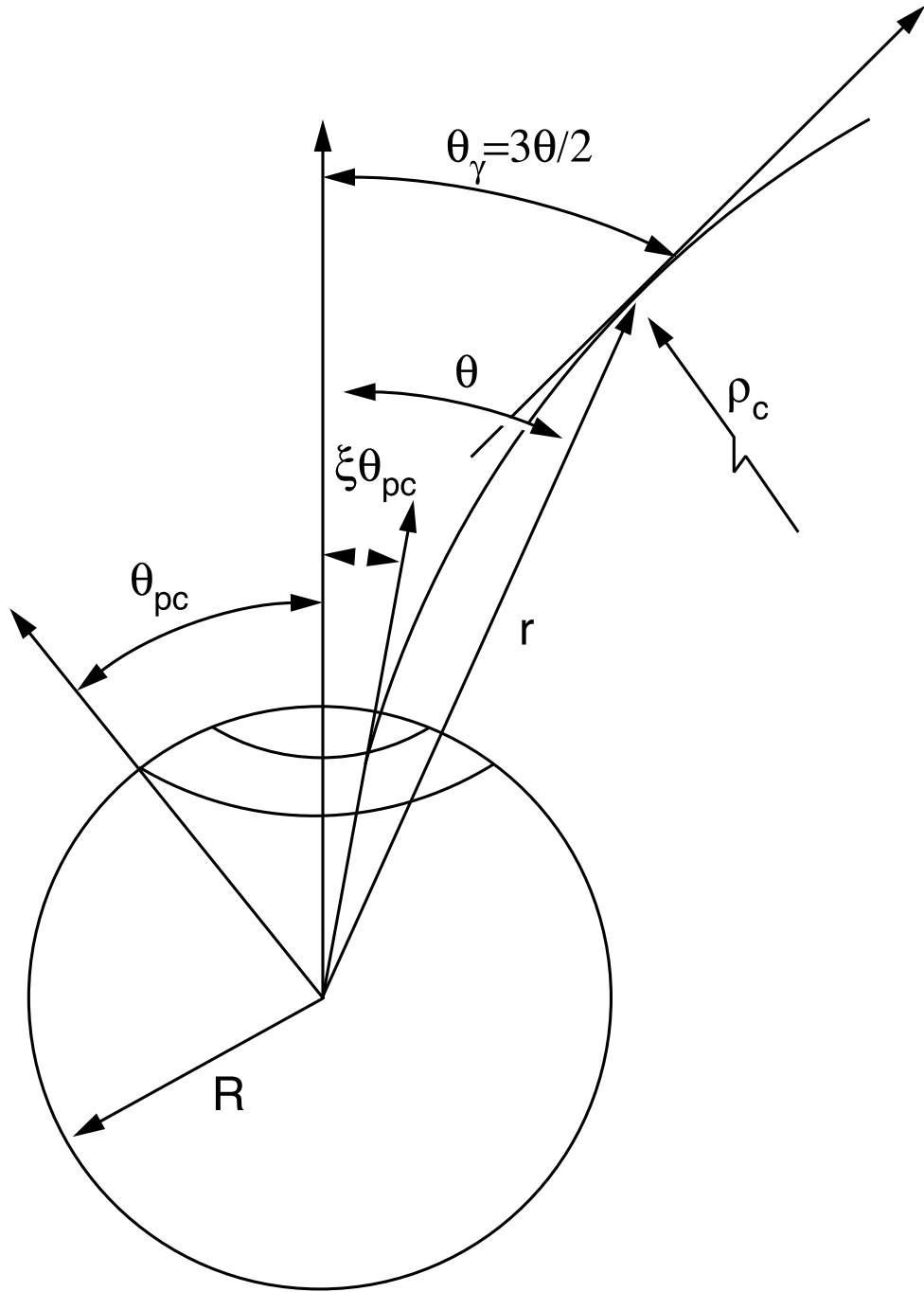


Fig. 3.— Geometry defining the angular quantities associated with a charged particle along an open field line defined by ξ emitting curvature radiation at θ and r along the line of sight, θ_γ .

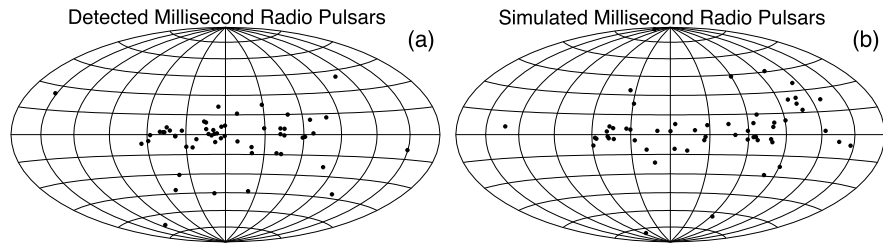


Fig. 4.— Aitoff projections of detected (a) and simulated (b) MSPs.

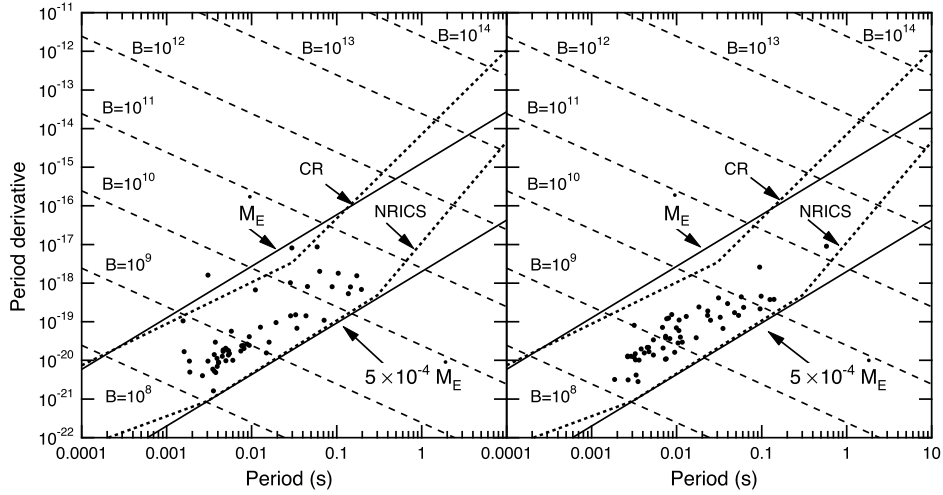


Fig. 5.— $\dot{P}-P$ diagram of millisecond pulsars detected (a) and simulated (b) by the group of ten radio surveys. The thin dashed lines represent the indicated traditional magnetic surface strength, assuming a constant dipole spin-down field. The dotted broken lines represent the pair death lines for curvature radiation (CR) and for nonresonant inverse Compton scattering (NRICS). The upper and lower MSPs birth lines for Eddington critical accretion rate \dot{M}_E (above) and $5 \times 10^{-4} \dot{M}_E$ of that rate (below) discussed in the text are indicated by solid lines.

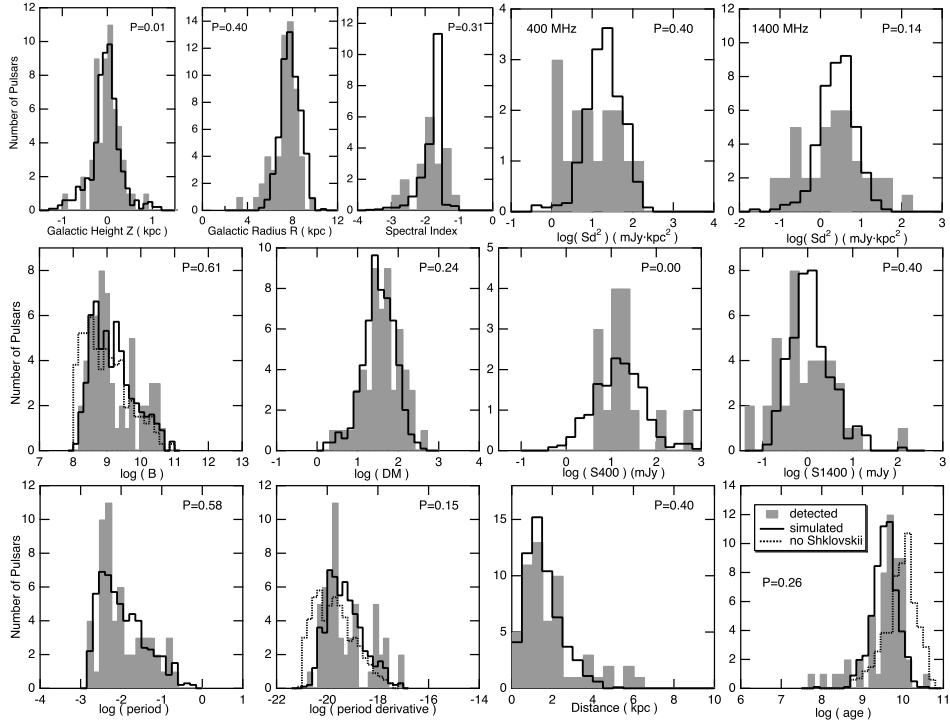


Fig. 6.— Distributions of various characteristics indicated for detected (shaded histograms) and simulated (unshaded histograms) MSPs from the Galactic disk. Also indicated is the p-value of the Kolmogorov-Smirnov test of the binned detected and simulated sample distributions at a significance level of $\alpha = 5\%$. The dotted histograms represent the simulated distributions without the Shklovskii effect.

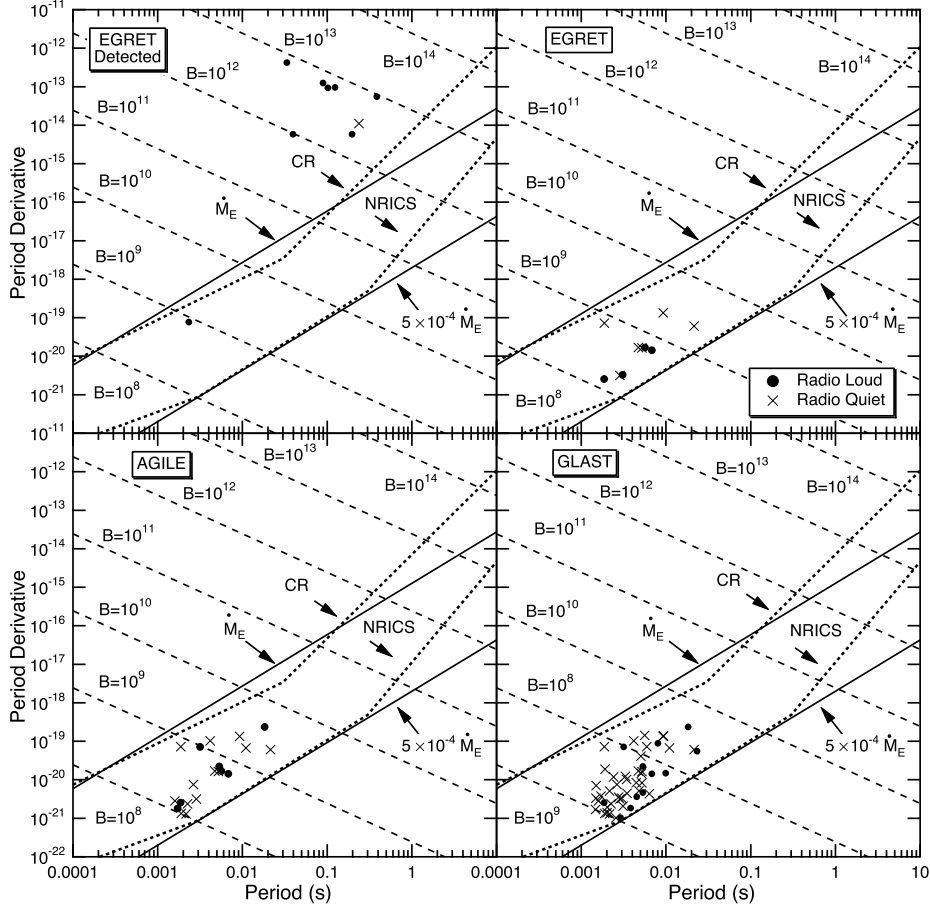


Fig. 7.— $\dot{P} - P$ diagram of radio-quiet (crosses) and radio-loud (solid circles) γ -ray normal and millisecond pulsars detected by EGRET (upper left) and millisecond pulsars predicted to be detected by EGRET (upper right), AGILE (lower left) and GLAST (lower right). The thin dashed lines represent the indicated traditional magnetic surface strength, assuming a constant dipole spin-down field. The dotted broken lines represent the pair death lines for curvature radiation (CR) and for nonresonant inverse Compton scattering (NRICS). The upper and lower MSPs birth lines for Eddington critical accretion rate \dot{M}_E (above) and $5 \times 10^{-4} \dot{M}_E$ of that rate (below) discussed in the text are indicated by solid lines.

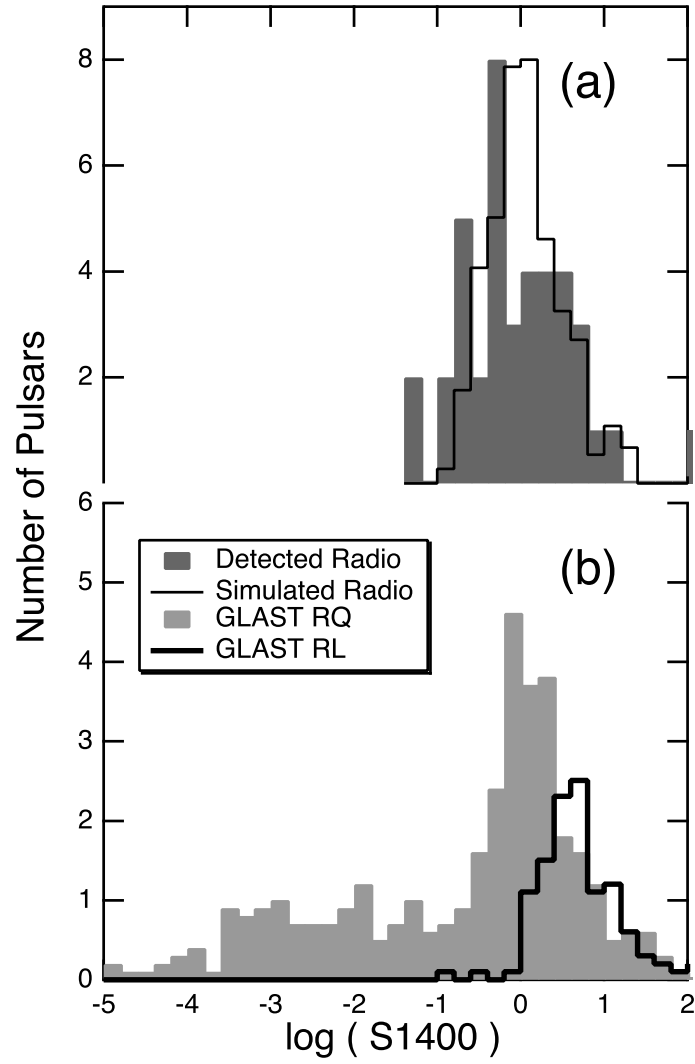


Fig. 8.— Radio flux at 1400 MHz plotted for detected and simulated radio pulsars in (a) and for GLAST radio-quiet and radio-loud γ -ray pulsars in (b).

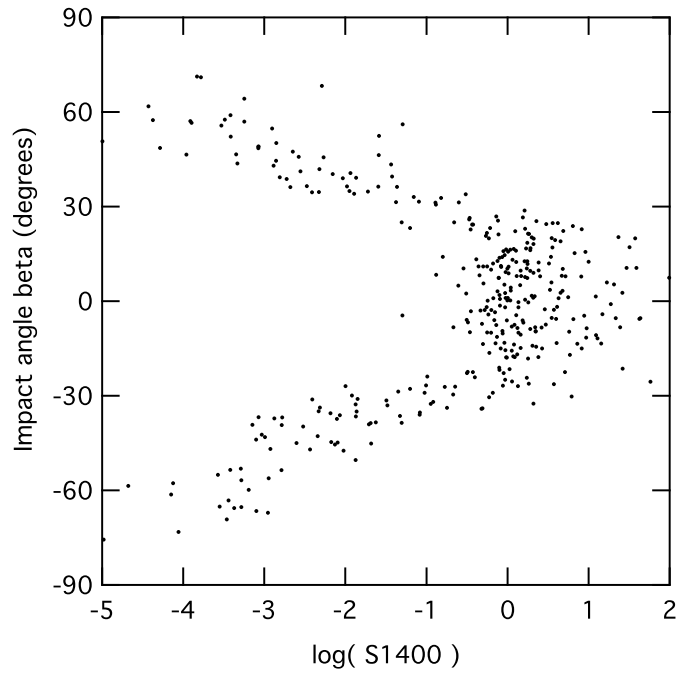


Fig. 9.— The impact angle β plotted as a function of the radio flux at 1400 MHz for the simulated GLAST radio-quiet γ -ray pulsars (10 times).

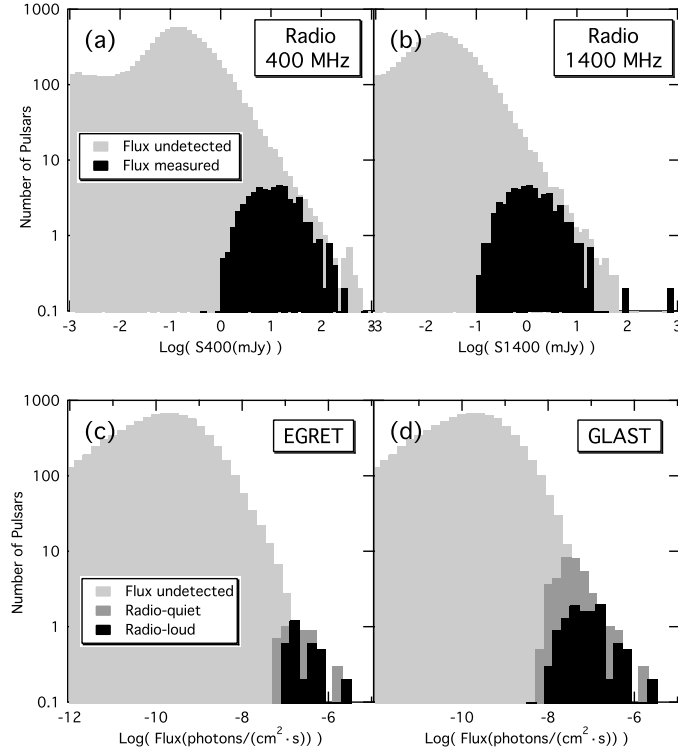


Fig. 10.— Log(N)-Log(S) for the radio flux at 400 MHz (a), 1400 MHz (b) and for EGRET (c) and GLAST (d). The light histograms represent the simulated undetected source counts. For the radio flux, the dark histograms indicated the simulated detected flux at 400 MHz (a) and 1400 MHz (b). For EGRET (c) and GLAST (d), the predicted γ -ray source counts are indicated for radio-loud (dark histograms) and radio-quiet (medium dark histograms) γ -ray millisecond pulsars.